Synoptic Meteorology Explains Temperate Forest Carbon Uptake

Nina A. Randazzo[1,2], Anna M. Michalak[1,2], and Ankur R. Desai[3]

1 Department of Global Ecology, Carnegie Institution for Science, Stanford, California, USA

2 Department of Earth System Science, Stanford University, Stanford, California, USA

3 Department of Atmospheric and Oceanic Sciences, University of Wisconsin-Madison, Madison, Wisconsin, USA

Corresponding author: Nina Randazzo (nrandazz@stanford.edu)

Key Points:

- Anomalously high temperatures, in addition to cloud cover, contribute to daily-scale suppression of net ecosystem productivity at forests in the Great Lakes region during nearby cyclonic precipitation events during the growing season.
- Forests in the Great Lakes region experience dampened growing season net ecosystem productivity during years in which this cyclonic system occurs frequently.
- Patterns of synoptic meteorology help inform regional net ecosystem productivity.

Abstract

While substantial attention has been paid to the effects of both global climate oscillations and local meteorological conditions on the interannual variability of ecosystem carbon exchange, the relationship between the interannual variability of synoptic meteorology and ecosystem carbon exchange has not been well studied. Here we use a clustering algorithm to identify a summertime cyclonic precipitation system northwest of the Great Lakes to determine a) the association at a daily scale between the occurrence of this system and the local meteorology and net ecosystem exchange at three Great Lakes region forested eddy covariance sites, and b) the association between the seasonal prevalence of this system and the summertime net ecosystem exchange of these sites. We find that temperature, in addition to precipitation and cloud cover, is an important explanatory factor for the suppression of net ecosystem productivity that occurs during these cyclonic events in this region. In addition, the prevalence of this cyclonic system can explain a significant proportion of the interannual variability in summertime forest ecosystem exchange in this region. This explanatory power is not due to a simple accumulation of low-productivity days that co-occur with this meteorological event, but rather a broader association between the frequency of these events and several aspects of prevailing seasonal conditions. This work demonstrates the usefulness of conceptualizing meteorology in terms of synoptic systems for explaining the interannual variability of regional carbon fluxes.

Plain Language Summary

Ecosystems exchange large amounts of carbon dioxide (CO_2) with the atmosphere. This rate of exchange is influenced by meteorological and climatological conditions. Because CO_2 is a major greenhouse gas, we need to determine the association between climate and ecosystem-atmosphere CO_2 exchange in order to understand potential climate feedbacks. Here we hypothesized that continental-scale atmospheric systems would be more informative than individual local meteorological variables for explaining the variability of regional carbon exchange, because these larger-scale systems concurrently indicate the state of several meteorological variables at various timescales, producing additive or interactive effects. We identified a particular summer storm system that leads to summertime rainfall and increased temperatures over and to the northwest of the Great Lakes. We found that the occurrence of this storm system is associated with weaker ecosystem carbon uptake at forests in the Great Lakes region. The widespread increase in temperature appears to contribute to this inhibition. A dampened seasonal cycle of carbon uptake is also associated with a high frequency of occurrence of this system. This work shows that large-scale weather patterns can help us understand how the ecosystem-atmosphere CO_2 exchange responds to climate.

1 Introduction

While the increasing trend in atmospheric CO_2 is primarily driven by fossil fuel emissions, the interannual variability is driven by the CO_2 exchange between the atmosphere and the terrestrial biosphere (e.g., Bousquet et al., 2000; Houghton, 2000; Knorr et al., 2007). Terrestrial carbon exchange is influenced at local to global scales by factors that include climate variability, land use change, CO_2 fertilization, and changes in nitrogen deposition (e.g., Ciais et al., 2019; Huntzinger et al., 2017). Feedbacks between climate variability and carbon uptake are still poorly understood (e.g., Friedlingstein et al., 2014; Knorr et al., 2007), because the mechanisms governing the interannual variability and carbon uptake remain uncertain.

The impact of annual to decadal oscillations in the climate system on terrestrial carbon uptake has been examined on local to global scales. For example, the effect of the phase of the El Niño-Southern Oscillation (ENSO) on global-scale photosynthesis and respiration, with ramifications for the global atmospheric CO_2 growth rate, has been particularly well studied (e.g., Gloor et al., 2018; Schwalm et al., 2011). These oscillations are themselves related to regional variability in multiple meteorological factors that may have additive or interactive effects on ecosystem carbon exchange (e.g., Jones et al., 2001; Knorr et al., 2007; Potter et al., 2003; Wharton et al., 2009).

In addition, the relationship between specific environmental drivers such as temperature, precipitation, or incoming radiation and carbon uptake has also been extensively explored, but the relationships have often been found to be heterogeneous in space and state-dependent. For example, both Fang et al. (2017) and Wang et al. (2014) found that the temperature sensitivity of large-scale biospheric carbon exchange depends upon other prevailing conditions, such as drought or ENSO phase. These findings suggest that various meteorological conditions do produce interacting effects on biospheric carbon exchange, and that global circulation indices are particularly informative in these state-dependent relationships.

The occurrence of specific synoptic meteorological systems may provide additional insight into drivers of variability in carbon uptake, but has received little attention. Synoptic meteorological patterns connect more directly to local conditions than do global climate oscillations, but still provide a link to large-scale atmospheric physics and, like climate oscillations, may influence several local variables at once. For example, regional circulation patterns in the Alps influence ecosystem productivity through their control of both temperature and precipitation seasonal anomalies, and are indicative of the state of the North Atlantic Oscillation and Arctic Oscillation (Desai et al., 2016). At finer temporal scales, decreased carbon uptake has been observed in North American ecosystems immediately before a summertime frontal passage, due to both intense cloud cover and high temperatures (e.g., Chan et al., 2004; Parazoo et al., 2008; Wang et al., 2007). In addition, observational and experimental data have shown outgassing of CO_2 from soil, particularly in relatively dry ecosystems, due to increased ecosystem respiration immediately following precipitation events (e.g., Birch et al., 1964; Unger et al., 2010).

Here, we explore the possibility that the occurrence of synoptic meteorological patterns may explain carbon uptake at local to regional, and at daily to interannual, scales. We focus on forests in the U.S. upper Midwest, where the role of climatic drivers of the variability of net carbon uptake has previously been examined using a variety of ecosystem carbon models (e.g., Chu et al., 2016; Desai et al., 2010a; Desai et al., 2010b; Wu et al., 2012). Such studies have produced valuable insights, but they have also highlighted an apparent state-dependence in the response of the carbon uptake to local meteorological variables, particularly on interannual scales.

The meteorological system of focus in the current analysis is summertime cyclonic activity associated with the interaction between the Great Plains Low Level Jet (GPLLJ) and the North American Jet. The GPLLJ itself is associated with significantly greater average growing season precipitation amount and intensity in the middle and northern Great Plains (Barandiaran et al., 2013; Weaver and Nigam, 2008). These effects on precipitation, particularly on heavy rainfall events, are due to the enhanced northward transport of warm moisture from the Gulf of Mexico to the central United States, where this process contributes to convective storms (Barandiaran et al., 2013; Weaver and Nigam, 2008). The placement and intensity of these precipitation events are influenced by an extratropical jet, hereafter referred to as the North American Jet, near the border between the United States and Canada. Although the North American Jet is an upper-level rather than a near-surface phenomenon, it is associated with a storm track that carries cyclones eastward and can lead to heavy precipitation in the summer over the Great Lakes region (e.g., Holman et al., 2014). As noted by Coleman and Budikova (2010) and Patricola et al. (2015), a strong GPLLJ that brings warm, moist air to an area experiencing cyclonic activity from the North American Jet can lead to extreme precipitation events where the outflow from the GPLLJ meets the cyclone. Models have suggested that global climate change will intensify the GPLLJ (Cook et al., 2008), such that any relationship between meteorological patterns and carbon uptake may be indicative of long-term trends in addition to interannual variability.

In the analysis that follows, we examine the frequency of occurrence of this meteorological feature and assess its relationship with daily to interannual variability in growing season carbon exchange at Midwestern forests, as exemplified by the University of Michigan Biological Station (US-UMB, Michigan), Park Falls (US-PFa, Wisconsin), and Willow Creek (US-WCr, Wisconsin) eddy covariance flux tower sites. While the GPLLJ is defined based on precipitation, its impact on carbon exchange may also be mediated through other meteorological variables. We

120 therefore also compare the observed impact of the examined meteorological feature to that of
121 individual meteorological variables such as precipitation, cloudiness, and temperature,
122 individually and in combination.

123 **2 Materials and Methods**

124 2.1 Identification of Synoptic Meteorological Systems

125 Meteorological reanalysis data were processed over North America for the years 1990 through
126 2014. We used the meteorological reanalysis CRU-NCEP gridded data processed as part of the
127 North American Carbon Project (NACP) MsTMIP biospheric model intercomparison data set
128 (for data through 2010: Wei et al., 2014; for data past 2010, Viovy, 2017). Data were organized
129 into a 1°×1° grid at a daily temporal resolution.

130 This daily gridded precipitation was sorted into regimes by a clustering algorithm, an
131 unsupervised machine learning method (see Text S1 for implementation details). Clustering
132 analyses involve sorting vectors in a large data set into groups based on distance between
133 vectors, generally without a priori assumptions about which patterns may emerge, in order to
134 identify distinct patterns in the data (Kaufman and Rousseeuw, 1990). We found that the spatial
135 characteristics of precipitation lend this meteorological variable particularly well to clustering
136 analyses. In this analysis, each grid cell over the domain for a given day is one dimension of the
137 precipitation vector for that day, as in other cluster analyses of meteorological fields (e.g., Bao
138 and Wallace, 2015; Cheng and Wallace, 1993; Fauchereau et al., 2009). Although this setup and
139 algorithm do not explicitly take into account the correlation between grid cells, the above-cited
140 authors have noted that the spatial correlation and physical coherence of meteorological systems
141 are preserved in clustering.

142 In order to obtain an index of the similarity of the precipitation at any given time to a given
143 precipitation pattern obtained through the clustering analysis, we used fuzzy rather than hard
144 clustering. In fuzzy clustering, rather than being assigned full membership to one cluster, data
145 points are assigned partial membership to different clusters. The strength of partial membership
146 of a given data point is described through a membership coefficient, with values ranging from 0
147 through 1. Classification of a data point into a given cluster as in hard clustering can still be
148 achieved simply by classifying the data point into the cluster for which the data point has the
149 greatest membership coefficient. This method was proposed and described in detail by Kaufman
150 and Rousseeuw (1990). The clustering analysis was carried out through the R function “fanny”
151 in the package “cluster” (Maechler et al., 2019) (see Text S1 for details).

152 This method can be used not only to classify individual days based on their dominant pattern of
153 precipitation, but also to characterize the meteorology of an entire month or season. For example,
154 if a particular 30-day month experiences a particular meteorological pattern frequently, that
155 month may contain six days during which a particular cluster describes the dominant
156 precipitation mechanism. Then, the membership coefficient for that cluster would be nearly 1 for
157 those six days, and therefore the mean membership coefficient would be approximately 0.2. This
158 number would indicate a greater dominance of this precipitation pattern during this month than
159 for another month that may have experienced this pattern as the dominant precipitation

mechanism for only one day, in which case the mean membership coefficient would be approximately 0.03.

2.2 Net Ecosystem Productivity

Daily-scale time series of NEE estimated using the eddy covariance method were obtained from FLUXNET2015 for the Great Lakes region forested sites at Park Falls (US-PFa; Berger et al., 2001; Desai, 2016a), the University of Michigan Biological Station (US-UMB; Gough et al., 2016; Schmid et al., 2003), and Willow Creek (US-WCr; Cook et al., 2004; Desai, 2016b) for June through August. While all three are considered forested sites, the footprint of US-PFa is heterogenous and also contains wetlands. All available years from 1996 to 2014 were used for each site. Local meteorological conditions, namely precipitation, air temperature, and incoming shortwave radiation, were also obtained for each site through the FLUXNET2015 database.

While NEE may include carbon dioxide fluxes from processes other than photosynthesis and ecosystem respiration (e.g., fire emissions, timber harvesting), NEE as measured by eddy covariance for the timescales and spatial scales investigated here are representative of photosynthesis and ecosystem respiration (Hayes et al., 2012). In the discussion that follows, we therefore assume that the measured flux represents net ecosystem productivity (NEP), and use NEP rather than NEE, in part because of the more intuitive sign convention that aids interpretability of carbon uptake in this context.

The 50th-percentile u* eddy covariance estimate of NEP was used. Data from years in which the average quality indicator of June through August daily NEP was below 0.8 (meaning that more than 20% of the data for an average day in the period was poor-quality gapfill) were discarded. This quality control resulted in five years of the US-PFa data and six years of the US-WCr data being removed.

2.3 Synthesis

The output from the meteorological clustering analysis was used in several ways. First, the clusters were examined, and a spatial pattern of summertime precipitation concentrated on the storm track of interest was identified. The physical mechanism of the spatial precipitation pattern was checked through an examination of the average atmospheric circulation on days classified into the cluster.

Then, the empirical probability density functions for fluxes and local meteorology at the study sites were compared between days experiencing the meteorological event of interest and other days in the season. The significance of associations between the occurrence of synoptic meteorological systems with local meteorological conditions and NEP was approximated using a t-test in the presence of approximate Gaussianity of the samples, or otherwise a Wilcoxon rank-sum test (see Text S3 for details). To determine whether anomalies in NEP observed during the meteorological event could be attributed to a simple additive relationship with mediating local conditions, NEP was regressed onto conditions that were themselves dependent on the meteorological event (e.g., temperature, cloudiness), and the residuals from the regression were tested for remaining dependency on the presence of the meteorological event.

Our attention then turned to the interannual association between the identified precipitation pattern and site-level fluxes. Both the synoptic precipitation variable and the carbon exchange variable at all sites were temporally divided into subsets of the summer season: June, July, August, June through July, July through August, and June through August. The correlation between all sub-seasonal subsets of the occurrence of the identified synoptic meteorological pattern and all sub-seasonal subsets of NEP was determined.

Potential mechanisms behind observed seasonal-scale relationships between the frequency of synoptic meteorological systems and carbon exchange were also investigated. For example, the synoptic event may be associated with a co-occurring change in a single local meteorological variable or a set of local variables, and the ecosystem may simply be responding to these local conditions during the event. These daily-scale carbon flux anomalies may then accumulate to produce any observed seasonal or annual anomaly. Alternatively, the frequency of occurrence of the synoptic system may be indicative of prevailing climatic anomalies that may influence NEP on longer timescales.

These potential mechanisms were first investigated through the previously-described correlation analysis as well as through a time series analysis. The correlation analysis across seasonal subsets (for example, June meteorology with July NEP) examined the possibility of a lag effect or association with longer-term climate forcing. In order to further investigate the distinction between cumulative daily effects versus longer-term seasonal effects, the time series of NEP were also orthogonally decomposed into components representing variability at different time scales using singular spectrum analysis (SSA). This method is especially well-suited for noisy and short time series of geophysical data such as ecosystem carbon flux, to determine the relative importance of anomalies in the seasonal cycle versus shorter-scale fluctuations for seasonal-scale carbon balance anomalies (Mahecha et al., 2007, 2010; Vautard et al., 1992; Figure S4) (see Text S2 for details). Clear differences in the seasonal cycle of carbon exchange, while not sufficient to rule out the importance of shorter-term responses, would be consistent with the hypothesis that the frequency of the synoptic event is associated with prevailing conditions that may affect ecosystem function on longer time scales.

To identify local variables that may mediate the associations between synoptic meteorology and NEP, several local variables were tested for significant correlations with the prevalence of synoptic systems. The local conditions that were found to be related to the synoptic systems were then regressed against NEP as the dependent variable (using the R package “leaps” by Lumley and Miller (2017)). If a linear combination of local conditions that are associated with a synoptic system can explain as much NEP variability as the synoptic system itself can, then this indicates that the mechanism linking the synoptic system to NEP may be a simple additive effect of these local conditions that are related to the occurrence of the synoptic event.

3 Results and Discussion

3.1 Identification of Summertime Cyclonic Precipitation Mechanism

One of the most dominant and consistently identified systems emerging from the cluster analysis was a cyclonic system associated with the intersection of the GPLLJ and the storm track associated with the jet stream. This system will be referred to here as the GLPF (Great Lakes

Precipitation Feature, Figure 1a). An examination of the tropospheric circulation associated with the GLPF supports the relevance of the GPLLJ and the storm track steered by the North American Jet in the generation of this system and the consistency of the physical mechanism that produces this precipitation pattern. The GLPF is associated with an anomalously strong cyclone to the northwest of the Great Lakes at the intersection of the GLPF and the jet stream (Figure 1c,d). In addition, the GLPF occurs almost exclusively during the growing season (Figure 1b), making it a good candidate for a meteorological feature that could impact NEP in the region with which it is associated.

3.2 Association Between Cyclonic System Occurrence and Net Ecosystem Productivity at the Daily Scale

We find that the GLPF is indeed associated with a significant reduction in carbon uptake during the summer (June through August) at all examined sites at the daily scale. The difference is significant based on a Wilcoxon rank sum test both for "raw" daily average NEP (Figure 2a,c,e, $p<0.01$ for all sites), and when carbon uptake data for each summer is normalized to eliminate interannual variability in mean uptake (results not shown).

The occurrence of the GLPF is associated with increased probabilities of precipitation and strong cloud cover in this region, as expected based on the definition of the GLPF. The occurrence of the GLPF nearly doubles the likelihood of the sites experiencing incoming shortwave radiation values in the severely limiting range (below 200 W m^{-2}) (Table 1). Similarly, precipitation is approximately twice as likely to occur during GLPF events (Table 1).

Although the GLPF is defined only based on precipitation, it is also associated with positive temperature anomalies in the Great Lakes region, and this association is unique for a summertime precipitation mechanism in this region. In the absence of the GLPF, summertime precipitation is associated with a slightly decreased mean temperature compared to dry summer days in this region ($p=7.3e-05$ for US-UMB, 0.0015 for US-PFa, 0.004 for US-WCr, based on a one-tailed t-test). However, during GLPF events, the temperature in this region is significantly elevated compared to non-GLPF days, regardless of the presence of local precipitation (Figure 3, $p<0.001$ for all sites). This positive temperature anomaly appears related to the strong southerly inflow associated with GLPF events (Figure 1d).

When the analysis is restricted to days experiencing neither precipitation nor severely limiting incoming shortwave radiation levels (Figure 2b,d,f) the difference in mean NEP between GLPF days and non-GLPF days decreases, indicating that much of this difference in NEP is due to the difference in the probability of limiting incoming shortwave radiation and precipitation. This conclusion is consistent with earlier studies that noted the decrease in net carbon uptake associated with rain events due to decreased photosynthesis that results from cloud cover, as noted by Chan et al. (2004). In drier ecoregions, the suppression of NEP during precipitation has also been linked to pulses of heterotrophic respiration associated with increased soil moisture, but this effect has not been shown to be relevant in this region (Birch et al., 1964; Unger et al., 2010).

All of the local meteorological associations, not just precipitation and cloud cover, must be taken into account to explain the full extent of NEP suppression in this region during GLPF events.

Despite the importance of local precipitation in the association between the GLPF and NEP suppression, a significant NEP suppression still exists at US-UMB and US-PFa during days experiencing neither precipitation nor severely limiting incoming shortwave radiation levels (Figure 2b,d). This effect even holds when the remaining effect of shortwave radiation limitation is eliminated (Figure 4a,c). The remaining NEP suppression associated with the GLPF can be largely explained by disproportionately high temperatures (Figure 4b,d). This apparent temperature effect is consistent with the findings of the case study of Wang et al. (2007), which linked high temperatures during summertime frontal passage to increased ecosystem respiration at US-PFa, and to both increased respiration and reduced photosynthesis in other North American ecosystems. However, this analysis shows the consistency of this temperature effect in explaining the full extent of NEP suppression during these synoptic events at sites in this region. The apparent temperature effect implies that the daily decrease in net carbon uptake during precipitation events can extend beyond the area of cloud cover and precipitation, depending on the physical mechanism causing the precipitation.

GLPF events produce anomalies in both photosynthesis and respiration through the alteration of several local meteorological conditions, as evidenced by a partioning of the eddy flux covariance NEP (see Text S4). A photosynthesis suppression associated with GLPF events appears to stem from the increased likelihood of limiting incoming shortwave radiation (Figure S1), while a respiration enhancement stems largely from positive temperature anomalies (Figures S2,3). This mechanism suggests that the NEP suppression seen in this region during GLPF events in the absence of associated cloud cover is due to respiration enhancement associated with anomalously high temperatures. However, at US-WCr, the enhancement is not statistically significant over days during which this site experiences no precipitation and greater than 200 W m^{-2} incoming shortwave radiation, consistent with the lack of significant NEP suppression at this site in the absence of precipitation and heavy cloud cover. This could be an indication of the relevance of precipitation for respiration at this site, although it should be noted that the sample size of this subset of GLPF days at this site is particularly small (23 days).

3.3 Association Between Cyclonic System Occurrence and Net Ecosystem Productivity at the Seasonal Scale

Beyond the daily association noted in the previous section, the July occurrence of the GLPF also explains region-wide reductions in summertime carbon uptake (Table S1, Figure 5) and in peak carbon uptake intensity (Figure S5). The prevalence of the GLPF in July correlates most significantly with July through August carbon uptake at all study sites (Table S1, Figure 5). The consistency of this relationship across sites suggests that GLPF-heavy midsummers are associated with regional depressions in carbon uptake. This relationship can also be viewed in terms of a relationship with peak growing season NEP (Figure S5), which was identified here using the isolated seasonal component from the time series orthogonal decomposition (Figure S4 and Text S2). Both NEP metrics show suppression during the years 1999 through 2002 and in 2010, years during which the GLPF occurred frequently during July (Figure 5b, Figure S5b).

The year 1998 is an outlier in the relationship between the July GLPF occurrence and July through August mean NEP (Figure 5a,b), but still follows the observed relationship between July GLPF occurrence and peak growing season NEP (Figure S5a,b). This disparity results from a strong peak NEP during the growing season of 1998, consistent with a low occurrence of GLPF

in July, immediately followed by a sharp decrease in NEP, leading to weak July through August mean NEP (Figure S4b).

The other year with complicated dynamics is 2001, when the weak uptake is consistent with the high occurrence of GLPF events during that year. This year also experienced a tent caterpillar outbreak that defoliated forests in the footprints of all three study sites (Cook et al., 2008), and it is not possible to determine the relative contributions of these two drivers, nor any possible causative relationship between the high occurrence of GLPF events that year and the caterpillar outbreak itself.

However, even if 2001 is eliminated from the analysis, a significant correlation remains between both peak and average July through August NEP and the July occurrence of GLPF events ($p<0.05$ at US-UMB and at US-PFa). At US-WCr, the exclusion of 2001 leaves only nine data points, reducing the power of the observed correlation ($p=0.13$).

We find that the relationship between July GLPF occurrence and July through August carbon uptake is more likely attributable to fluctuations in NEP seasonal cycle amplitude rather than simply to the cumulative impacts of daily-scale responses on days experiencing GLPF events. As already stated, the July GLPF correlates best with July through August (rather than just July) NEP across sites (Table S1). While this does not necessarily disprove the importance of the daily-scale response, it at least suggests that if the daily scale response is important in this relationship, then there must be a persistent effect associated with this daily response, and the interannual relationship is not simply due to the sum of negative carbon uptake anomalies during individual GLPF events. Indeed, the years with decreased net July through August carbon uptake show a dampened peak in the seasonal component of the NEP time series, with suppression often becoming apparent before the start of July. This suggests that reduced July through August uptake may be related to conditions that occur earlier in the season (Figure 6). The importance of NEP intensity as opposed to growing season length for the interannual variability of ecosystem carbon balance is consistent with the findings of Fu et al. (2019) and Zscheischler et al. (2016), and the work presented here further highlights the importance of the seasonal-scale rather than only daily-scale NEP intensity.

The explanatory power of GLPF July frequency for NEP interannual variability seems to stem from its relationship to both daily-scale conditions directly related to GLPF events and longer-term meteorological forcing indirectly related to these events, which together may influence the intensity and seasonal characteristics of NEP. Site-specific temperature, precipitation, and incoming shortwave radiation during subsets of the growing season correlate significantly ($p<0.05$) with the July occurrence of GLPF events at one or more sites (Table 2). These variables include June conditions, consistent with the idea that differences in NEP intensity during high-GLPF years seem to emerge before the start of July (Figure 6).

A statistical analysis provides clues regarding the nature of the GLPF-NEP relationship at long timescales. Restricting the analysis to growing season local meteorology as potential mediating conditions, we see that at the Wisconsin sites, a combination of a GLPF-correlated temperature variable during cloudy or wet days during July or during June through July with a GLPF-correlated incoming shortwave radiation variable in June explains as much or more of the variability in July to August NEP as does the July occurrence of GLPF events (Table 3). These

results suggest that while the establishment of a mechanistic relationship would require further study, the observed relationships between GLPF and NEP at the Wisconsin sites may be due to the additive effects of anomalously warm cloudy or wet days and heavy cloud cover, the latter preceding July GLPF activity.

However, at US-UMB, the GLPF correlates only with precipitation variables, none of which correlate significantly with July through August NEP (Tables 2, 3). Further, when the same model selection process is conducted with standardized and pooled NEP and local conditions across sites, the resulting model cannot explain nearly as much variability in July through August NEP as can the GLPF (Table 3).

Thus, the region-wide variability associated with the July occurrence of the GLPF cannot be adequately explained by linear combinations of local meteorological variables that co-occur with the GLPF. Additive effects of growing season conditions alone cannot explain the NEP suppression that tends to be experienced across forests in this region during summers with prevalent GLPF activity. In addition, even at the Wisconsin sites, meteorological forcing from earlier in the season (June incoming shortwave radiation anomalies) rather than only co-occurring meteorological conditions appear relevant for July through August NEP.

It is possible that teleconnections that relate winter and early spring conditions to the frequency of the July GLPF may affect growing season NEP or the response of growing season NEP to co-occurring local meteorology. This idea is consistent with the findings of Wolf et al. (2016) and Zscheischler et al. (2016), who showed, respectively, that strong NEP cannot be explained solely by co-occurring meteorology and that conditions early in the springtime may alter NEP responses to conditions later in the growing season. Further research is needed to test for such mechanisms.

In summary, GLPF occurrence on the seasonal scale remains unique in its ability to explain a significant amount of variability across this region in summertime. The frequency of synoptic systems may indicate meteorological conditions on multiple timescales, potentially providing information about ecosystem response.

4 Conclusions

The analysis presented here demonstrates that the frequency of occurrence of specific synoptic meteorological systems may be a powerful and thus far untapped indicator of interannual variability in carbon uptake.

For the temperate forests located in the U.S. upper Midwest examined here, the occurrence of the GLPF appears to be directly related to ecosystem carbon exchange at daily and seasonal scales. At the daily scale, the occurrence of this precipitation system seems to suppress NEP not only through cloud cover and precipitation, but also through significantly increased temperatures outside of the clouded region. The NEP suppression observed in the presence of heavy cloud cover and precipitation is primarily associated with a suppression of photosynthesis, whereas respiration enhancements occur outside of the clouded area due to the positive temperature anomaly associated with the GLPF circulation. This result demonstrates the importance of the GLPF in relating precipitation events to fluctuations in NEP in this region. The temperature

406 relationship serves as a mechanism that may lead to NEP suppression outside of the area of cloud
407 cover. This mechanism is highly dependent on the physical mechanism of the precipitation
408 system, as most summertime precipitation events in this region are not associated with any
409 temperature enhancement.

410 At seasonal and interannual scales, the prevalence of the GLPF explains the interannual
411 variability of midsummer NEP across all forested sites in the study better than any individual
412 meteorological variables or simple combinations thereof. This relationship does not seem to be
413 due only to an accumulation of daily-scale responses to July GLPF events, but rather is
414 indicative of alterations to the overall seasonal cycle of NEP. Furthermore, the mechanism does
415 not manifest itself uniformly across the examined region. For example, at the Michigan site,
416 additive effects of local conditions associated with high GLPF prevalence cannot fully explain
417 the relationship, but the reverse is true at the Wisconsin sites.

418 Further research is needed to understand the association between the frequency of synoptic
419 events such as the GLPF and large-scale climate conditions that may affect the seasonal cycle of
420 carbon exchange.

Acknowledgments, Samples, and Data

This study was supported by the Atmospheric Carbon and Transport (ACT) - America project, which is a NASA Earth Venture Suborbital 2 project funded by NASA's Earth Science Division (Grant NNX15AJ42G to the Carnegie Institution for Science). A. R. Desai acknowledges support from DOE Ameriflux Network Management Project award to ChEAS core site cluster

This work used eddy covariance data acquired and shared by the FLUXNET community, specifically from the AmeriFlux network. The ERA-Interim reanalysis data are provided by ECMWF and processed by LSCE. The FLUXNET eddy covariance data processing and harmonization was carried out by the European Fluxes Database Cluster, AmeriFlux Management Project, and Fluxdata project of FLUXNET, with the support of CDIAC and ICOS Ecosystem Thematic Center, and the OzFlux, ChinaFlux and AsiaFlux offices. The FLUXNET2015 data from the sites used in this study are listed under https://doi.org/10.18140/FLX/1440089 (US-PFa), https://doi.org/10.18140/FLX/1440095 (US-WCr), and https://doi.org/10.18140/FLX/1440093 (US-UMB). US-PFa and US-WCr are sponsored by the DOE AmeriFlux Network Management Project and NOAA/ESRL. US-UMB is sponsored by the DOE AmeriFlux Network Management Project, NOAA, NICCR, and the NSF.

Gridded CRU-NCEP MsTMIP driver reanalysis precipitation and vector winds through 2010 were obtained through Oak Ridge National Laboratory's data repository at https://doi.org/10.3334/ORNLDAAC/1220.

Gridded CRU-NCEP MsTMIP driver reanalysis precipitation and vector winds that extended beyond 2010 were made available by Nicolas Viovy of IPS-Laplace at https://vesg.ipsl.upmc.fr/thredds/catalog/work/p529viov/cruncep/V8_1901_2016/catalog.html.

Statistical analyses were performed using the R "stats" and "base" packages. Clustering was performed using the R "cluster" package. Model selection was performed using the R "leaps" package. The R software and all R packages are open source and can be found at https://cran.r-project.org/.

Mapping was performed using the open source "m_map" package (https://www.eoas.ubc.ca/~rich/map.html) in MATLAB (https://www.mathworks.com).

References

Bao, M., & Wallace, J. M. (2015), Cluster analysis of Northern Hemisphere wintertime 500-hPa flow regimes during 1920–2014, *Journal of the Atmospheric Sciences*, *72*(9), 3597-3608, https://doi.org/10.1175/jas-d-15-0001.1

Barandiaran, D., Wang, S., & Hilburn, K. (2013), Observed trends in the Great Plains low-level jet and associated precipitation changes in relation to recent droughts, *Geophysical Research Letters*, *40*(23), 6247-6251, https://doi.org/10.1002/2013GL058296

Berger, B. W., Davis, K. J., Yi, C., Bakwin, P. S., & Zhao, C. L. (2001), Long-term carbon dioxide fluxes from a very tall tower in a northern forest: Flux measurement methodology, *Journal of Atmospheric and Oceanic Technology*, *18*(4), 529-542, https://doi.org/10.1175/1520-0426(2001)018<0529:ltcdff>2.0.co;2

Birch, H. F. (1964), Mineralisation of plant nitrogen following alternate wet and dry conditions, *Plant and Soil*, *20*(1), 43-49, https://doi.org/10.1007/bf01378096

Bousquet, P., Peylin, P., Ciais, P., Le Quere, C., Friedlingstein, P., & Tans, P. P. (2000), Regional changes in carbon dioxide fluxes of land and oceans since 1980, *Science*, *290*(5495), 1342-1346, https://doi.org/10.1126/science.290.5495.1342

Chan, D., Yuen, C. W., Higuchi, K., Shashkov, A., Liu, J., Chen, J., & Worthy, D. (2004), On the CO2 exchange between the atmosphere and the biosphere: the role of synoptic and mesoscale processes, *Tellus Series B-Chemical and Physical Meteorology*, *56*(3), 194-212, https://doi.org/10.1111/j.1600-0889.2004.00104.x

Cheng, X., & Wallace, J. M. (1993), Cluster analysis of the Northern Hemisphere wintertime 500-hPa height field: Spatial patterns, *Journal of the Atmospheric Sciences*, *50*(16), 2674-2696, https://doi.org/10.1175/1520-0469(1993)050<2674:caotnh>2.0.co;2

Chu, H., Chen, J., Gottgens, J. F., Desai, A. R., Ouyang, Z., & Qian, S. S. (2016), Response and biophysical regulation of carbon dioxide fluxes to climate variability and anomaly in contrasting ecosystems in northwestern Ohio, USA, *Agricultural and Forest Meteorology*, *220*, 50-68, https://doi.org/10.1016/j.agrformet.2016.01.008

Coleman, J. S. M., & Budikova, D. (2010), Atmospheric aspects of the 2008 Midwest floods: a repeat of 1993?, *International Journal of Climatology*, *30*(11), 1645-1667, https://doi.org/10.1002/joc.2009

Cook, B. D., Bolstad, P. V., Martin, J. G., Heinsch, F. A., Davis, K. J., Wang, W., Desai, A. R., & Teclaw, R. M. (2008), Using light-use and production efficiency models to predict photosynthesis and net carbon exchange during forest canopy disturbance, *Ecosystems*, *11*(1), 26-44, https://doi.org/10.1002/joc.200910.1007/s10021-007-9105-0

Cook, B. D., Davis, K. J., Wang, W., Desai, A. R., Berger, B. W., Teclaw, R. M., et al. (2004), Carbon exchange and venting anomalies in an upland deciduous forest in northern Wisconsin,

485 USA, *Agricultural and Forest Meteorology*, *126*(3), 271-295,
486 https://doi.org/10.1016/j.agrformet.2004.06.008

487 Cook, K., Vizy, E., Launer, Z., & Patricola, C. (2008), Springtime intensification of the Great
488 Plains Low-Level Jet and Midwest precipitation in GCM simulations of the twenty-first
489 century, *Journal of Climate*, *21*(23), 6321-6340, https://doi.org/10.1175/2008JCLI2355.1

490 Desai, A. R. (2010), Climatic and phenological controls on coherent regional interannual
491 variability of carbon dioxide flux in a heterogeneous landscape, *Journal of Geophysical*
492 *Research: Biogeosciences*, *115*(G3), https://doi.org/10.1029/2010JG001423

493 Desai, A. R. (2016a), FLUXNET2015 US-PFa Park Falls/WLEF,
494 https://doi.org/10.18140/FLX/1440089

495 Desai, A. R. (2016b), FLUXNET2015 US-WCr Willow Creek,
496 https://doi.org/10.18140/FLX/1440095

497 Desai, A. R., Helliker, B. R., Moorcroft, P. R., Andrews, A. E., & Berry, J. A. (2010), Climatic
498 controls of interannual variability in regional carbon fluxes from top-down and bottom-up
499 perspectives, *Journal of Geophysical Research: Biogeosciences*, *115*(G2),
500 https://doi.org/10.1029/2009JG001122

501 Desai, A. R., Wohlfahrt, G., Zeeman, M. J., Katata, G., Eugster, W., Montagnani, L., et al.
502 (2016), Montane ecosystem productivity responds more to global circulation patterns than
503 climatic trends, *Environmental Research Letters*, *11*(2), https://doi.org/10.1088/1748-
504 9326/11/2/024013

505 Chan, D., and Yuen, C.-W., Higuchi, K., Shashkov, A., Liu, J., Chen, J., & Worthy, D. (2004),
506 On the CO_2 exchange between the atmosphere and the biosphere: the role of synoptic and
507 mesoscale processes, *Tellus B: Chemical and Physical Meteorology*, *56*(3), 194-212,
508 https://doi.org/10.3402/tellusb.v56i3.16424

509 Fang, Y., Michalak, A. M., Schwalm, C. R., Huntzinger, D. N., Berry, J. A., Ciais, P., et al.
510 (2017), Global land carbon sink response to temperature and precipitation varies with ENSO
511 phase, *Environmental Research Letters*, *12*(6), https://doi.org/10.1088/1748-9326/aa6e8e

512 Fauchereau, N., Pohl, B., Reason, C. J. C., Rouault, M., & Richard, Y. (2009), Recurrent daily
513 OLR patterns in the Southern Africa/Southwest Indian Ocean region, implications for South
514 African rainfall and teleconnections, *Climate Dynamics*, *32*(4), 575-591,
515 https://doi.org/10.1007/s00382-008-0426-2

516 Friedlingstein, P., Meinshausen, M., Arora, V. K., Jones, C. D., Anav, A., Liddicoat, S. K., &
517 Knutti, R. (2014), Uncertainties in CMIP5 climate projections due to carbon cycle
518 feedbacks, *Journal of Climate*, *27*(2), 511-526, https://doi.org/10.1175/jcli-d-12-00579.1

519 Fu, Z., Stoy, P. C., Poulter, B., Gerken, T., Zhang, Z., Wakbulcho, G., & Niu, S. (2019),
520 Maximum carbon uptake rate dominates the interannual variability of global net ecosystem
521 exchange, *Global Change Biology*, *25*(10), 3381-3394, https://doi.org/10.1111/gcb.14731

Gloor, E., Wilson, C., Martyn, P. C., Chevallier, F., Buermann, W., & Boesch, H., et al. (2018), Tropical land carbon cycle responses to 2015/16 El Niño as recorded by atmospheric greenhouse gas and remote sensing data, *Philosophical Transactions of the Royal Society B: Biological Sciences*, *373*(1760), https://doi.org/10.1098/rstb.2017.0302

Gough, C., Bohrer, G., & Curtis, P. (2016), FLUXNET2015 US-UMB Univ. of Mich. Biological Station, https://doi.org/10.18140/FLX/1440093

Hayes, D., & Turner, D. (2012), The need for "apples-to-apples" comparisons of carbon dioxide source and sink estimates, *Eos, Transactions American Geophysical Union*, *93*(41), 404-405, https://doi.org/10.1029/2012eo410007

Holman, K. D., Lorenz, D. J., & Notaro, M. (2014), Influence of the background state on rossby wave propagation into the Great Lakes region based on observations and model simulations, *Journal of Climate*, *27*(24), 9302-9322, https://doi.org/10.1175/jcli-d-13-00758.1

Houghton, R. A. (2000), Interannual variability in the global carbon cycle, *Journal of Geophysical Research-Atmospheres*, *105*(D15), 20121-20130, https://doi.org/10.1029/2000jd900041

Jones, C. D., Collins, M., Cox, P. M., & Spall, S. A. (2001), The carbon cycle response to ENSO: a coupled climate–carbon cycle model study, *Journal of Climate*, *14*(21), 4113-4129, https://doi.org/10.1175/1520-0442(2001)014<4113:tccrte>2.0.co;2

Kaufman, L., & Rousseeuw, P. J. (1990), Chapter 4: Fuzzy Analysis (Program FANNY), in *Finding Groups in Data: An Introduction to Cluster Analysis*, Hoboken, New Jersey: John Wiley & Sons, Inc.

Knorr, W., Gobron, N., Scholze, M., Kaminski, T., Schnur, R., & Pinty, B. (2007), Impact of terrestrial biosphere carbon exchanges on the anomalous CO_2 increase in 2002-2003, *Geophysical Research Letters*, *34*(9), 6, https://doi.org/10.1029/2006gl029019

Lumley, T., & Miller, A. (2017), leaps: Regression Subset Selection, R package.

Maechler, M., Rousseeuw, P., Struyf, A., Hubert, M., & Hornik, K. (2019), cluster: Cluster Analysis Basics and Extensions, R package.

Mahecha, M. D., Reichstein, M., Jung, M., Seneviratne, S. I., Zaehle, S., Beer, C., et al. (2010), Comparing observations and process-based simulations of biosphere-atmosphere exchanges on multiple timescales, *Journal of Geophysical Research: Biogeosciences (2005–2012)*, *115*(G2), https://doi.org/10.1029/2009JG001016

Mahecha, M. D., Reichstein, M., Lange, H., Carvalhais, N., Bernhofer, C., Grünwald, T., Papale, D., & Seufert, G. (2007), Characterizing ecosystem-atmosphere interactions from short to interannual time scales, *Biogeosciences*, *4*(5), 743-758, https://doi.org/10.5194/bg-4-743-2007

Parazoo, N. C., Denning, A. S., Kawa, S. R., Corbin, K. D., Lokupitiya, R. S., & Baker, I. T. (2008), Mechanisms for synoptic variations of atmospheric CO_2 in North America, South

America and Europe, *Atmos. Chem. Phys.*, *8*(23), 7239-7254, https://doi.org/10.5194/acp-8-7239-2008

Patricola, C. M., Chang, P., & Saravanan, R. (2015), Impact of Atlantic SST and high frequency atmospheric variability on the 1993 and 2008 Midwest floods: Regional climate model simulations of extreme climate events, *Climatic Change*, *129*(3-4), 397-411, https://doi.org/10.1007/s10584-013-0886-1

Potter, C., Klooster, S., Steinbach, M., Tan, P., Kumar, V., Shekhar, S., Nemani, R., & Myneni, R. (2003), Global teleconnections of climate to terrestrial carbon flux, *Journal of Geophysical Research: Atmospheres (1984–2012)*, *108*(D17), https://doi.org/10.1029/2002JD002979

R Core Team (2019), R: A Language and Environment for Statistical Computing.

Schmid, H. P., Su, H.-B., Vogel, C. S., & Curtis, P. S. (2003), Ecosystem-atmosphere exchange of carbon dioxide over a mixed hardwood forest in northern lower Michigan, *Journal of Geophysical Research: Atmospheres*, *108*(D14), https://doi.org/10.1029/2002jd003011

Schwalm, C. R., Williams, C. A., Schaefer, K., Baker, I., Collatz, G. J., & Rödenbeck, C. (2011), Does terrestrial drought explain global CO_2 flux anomalies induced by El Niño?, *Biogeosciences*, *8*(9), 2493-2506, https://doi.org/10.5194/bg-8-2493-2011

Schwarz, G. (1978), Estimating the Dimension of a Model, *The Annals of Statistics*, *6*(2), 461-464.

Unger, S., Máguas, C., Pereira, J. S., David, T. S., & Werner, C. (2010), The influence of precipitation pulses on soil respiration – Assessing the "Birch effect" by stable carbon isotopes, *Soil Biology and Biochemistry*, *42*(10), 1800-1810, https://doi.org/10.1016/j.soilbio.2010.06.019

Vautard, R., Yiou, P., & Ghil, M. (1992), Singular-spectrum analysis: A toolkit for short, noisy chaotic signals, *Physica D: Nonlinear Phenomena*, *58*(1), 95 - 126, https://doi.org/10.1016/0167-2789(92)90103-T

Viovy, N. (2017), CRU-NCEP Reanalysis Dataset, Version 8, IPS-Laplace.

Wang, J.-W., Denning, A. S., Lu, L., Baker, I. T., Corbin, K. D., & Davis, K. J. (2007), Observations and simulations of synoptic, regional, and local variations in atmospheric CO_2, *Journal of Geophysical Research-Atmospheres*, *112*(D4), https://doi.org/10.1029/2006jd007410

Wang, X., Piao, S., Ciais, P., Friedlingstein, P., Myneni, R. B., Cox, P., et al. (2014), A two-fold increase of carbon cycle sensitivity to tropical temperature variations, *Nature*, *506*, 212, https://doi.org/10.1038/nature12915

Weaver, S., & Nigam, S. (2008), Variability of the great plains low-level jet: Large-scale circulation context and hydroclimate impacts, *Journal of Climate*, *21*(7), 1532-1551, https://doi.org/10.1175/2007JCLI1586.1

Wei, Y., Liu, S., Huntzinger, D. N., Michalak, A. M., Viovy, N., Post, W. M. et al. (2014), NACP MsTMIP: Global and North American driver data for multi-model intercomparison. Oak Ridge National Laboratory Distributed Active Archive Center, Oak Ridge, Tennessee, USA. http://dx.doi.org/10.3334/ORNLDAAC/1220

Wharton, S., Chasmer, L., Falk, M., & Paw U, K. T. (2009), Strong links between teleconnections and ecosystem exchange found at a Pacific Northwest old-growth forest from flux tower and MODIS EVI data, *Global Change Biology*, 15(9), 2187-2205, https://doi.org/10.1111/j.1365-2486.2009.01952.x

Wolf, S., Keenan, T. F., Fisher, J. B., Baldocchi, D. D., Desai, A. R., Scott, R. L., Law, B. E., et al. (2016), Warm spring reduced carbon cycle impact of the 2012 US summer drought, *Proceedings of the National Academy of Sciences,* (113)21, 5880-5885, https://doi.org/ 10.1073/pnas.1519620113

Wu, J., van der Linden, L., Lasslop, G., Carvalhais, N., Pilegaard, K., Beier, C., & Ibrom, A. (2012), Effects of climate variability and functional changes on the interannual variation of the carbon balance in a temperate deciduous forest, *Biogeosciences*, *9*(1), 13-28, https://doi.org/10.5194/bg-9-13-2012

Zscheischler, J., Fatichi, S., Wolf, S., Blanken, P. D., Bohrer, G., Clark, K., et al. (2016), Short-term favorable weather conditions are an important control of interannual variability in carbon and water fluxes, *Journal of Geophysical Research: Biogeosciences*, *121*(8), 2186-2198, https://doi.org/10.1002/2016JG003503

614 **Table 1:** For all sites, the occurrence of the GLPF approximately doubles the likelihood of precipitation
615 (P>0 mm) and of severely limiting incoming shortwave radiation (R<200 W m^{-2}) on the daily scale for

	Likelihood of P > 0 mm		**Likelihood of R < 200 W m^{-2}**	
Site	GLPF	No GLPF	GLPF	No GLPF
US-UMB	0.65	0.33	0.44	0.25
US-PFa	0.63	0.31	0.60	0.32
US-WCr	0.68	0.34	0.52	0.25

616 the months of June through August.

617

618 **Table 2:** Site-specific variables, among those listed in Table S2, that are significantly (p<0.05, denoted by
619 gray shading) correlated to the prevalence of GLPF in July. Among these, none were significantly
620 correlated with July through August US-UMB NEP, five were significantly correlated with US-PFa NEP,
621 and one was significantly correlated with US-WCr NEP (the significance cutoff was raised to p<0.1 for
622 NEP correlations because of more limited NEP data availability at this site). The coefficient of
623 determination (R^2) is shown for GLPF-correlated (shaded) variables significantly correlated to July-
624 August NEP at each site.
625

Category	Variables	US-UMB	US-PFa	US-WCr
Temperature	$T_{p>0,\ p=0.25,\ July}$		R^2=0.39	
	$T_{p>0,\ p=0.50,\ July}$		R^2=0.28	
	$T_{R<200,\ p=0.25,\ July}$			
	$T_{R<200,\ p=0.75,\ June\text{-}July}$			R^2=0.33
	$T_{R<200,\ p=0.50,\ June\text{-}August}$			
	$T_{R<200,\ p=0.50,\ July\text{-}August}$			
Incoming shortwave radiation	$R_{p=0.50,\ June}$		R^2=0.28	
	$R_{p=0.75,\ June}$			
	$n_{R<200,\ June}$			
	$R_{p=0.50,\ July}$			
	$R_{p=0.75,\ July}$		R^2=0.24	
	$R_{p=0.75,\ June\text{-}July}$			
	$R_{p=0.75,\ July\text{-}August}$			
	$R_{p=0.75,\ June\text{-}August}$			
Precipitation	P_{June}			
	$n_{P>0,\ June}$			
	$n_{P>5,\ June}$			
	P_{July}		R^2=0.21	
	$P_{June\ -\ July}$			
	$n_{P>5,\ June\text{-}July}$			
	$P_{June\text{-}August}$			
	$n_{P>5,\ June\text{-}August}$			

626

627 **Table 3:** Variables that best explain mean July-August NEP at each site and across sites. For each site,
628 the variables eligible for selection were constrained to only variables that were significantly (p<0.05)
629 correlated with the July occurrence of GLPF at that particular site (see shaded cells in Table 2). Up to two
630 variables were selected, but no two variables that included overlapping data were allowed. A two-variable
631 model is only shown for cases where the two-variable model outperformed the one-variable model based
632 on the Bayesian Information Criterion [*Schwarz*, 1978]. The top row shows the R^2 between the July
633 occurrence of GLPF and the mean July through August NEP for comparison.

	Pooled	**US-UMB**	**US-PFa**	**US-WCr**
GLPF	GLPF (R^2=0.44)	GLPF (R^2=0.48)	GLPF (R^2=0.38)	GLPF (R^2=0.50)
1 variable	$T_{P>0,\ p=0.25,\ July}$ (R^2=0.12)	*N/A*	$T_{P>0,\ p=0.25,\ July}$ (R^2=0.39)	$T_{R<200,\ p=0.75,\ June\text{-}July}$ (R^2=0.33)
2 variables	*N/A*	*N/A*	$T_{P>0,\ p=0.50,\ July}$, $R_{p=0.50,\ June}$ (R^2= 0.59)	$T_{R<200,\ p=0.75,\ June\text{-}July}$, $R_{p=0.50,\ June}$ (R^2= 0.55)

634
635

Figure 1: The GLPF precipitation cluster is a synoptic meteorological pattern centered around the upper Midwest and consistently associated with a mid-latitude cyclone resulting from an interaction between the Great Plains Low Level Jet and the North American Jet Stream. Triangles denote tower locations. (a): The map of average daily precipitation [mm] associated with the GLPF at 1°×1° resolution shows enhanced precipitation over and to the northwest of the Great Lakes, with trails of precipitation from the southerly and northwesterly directions. (b): The GLPF occurs primarily during the summer. (c): The average vector winds associated with the GLPF reveal the mechanism behind this precipitation system, with a strong Great Plains Low Level Jet, strong northwesterly circulation associated with the North American Jet Stream, and a cyclone in the region of enhanced precipitation (which is also the region where these two circulation systems meet). (d): The anomaly of average vector winds associated with the GLPF from June to August compared to all other days in this time of year highlights the GLPF-related circulation anomaly.

Figure 2: At (a) US-UMB, (c) US-PFa, and (e) US-WCr, days experiencing a GLPF event in June through August (light gray box plots) have significantly lower daily NEP relative to days not experiencing a GLPF event (dark grey box plots), according to a Wilcoxon rank sum test of the difference between the population means. When the analysis is restricted to days not experiencing precipitation (P = 0 mm) or heavy cloud cover (R < 200 W m^{-2}), the NEP suppression is reduced but remains significant at (b) US-UMB and (d) US-PFa. At (f) WCr, the suppression is no longer significant, indicating that the suppression at this site associated with the GLPF may be entirely due to the increased probability of precipitation and heavy cloud cover. In all panels, n indicates the number of days considered and p is the p-value from the hypothesis test comparing the GLPF and non-GLPF days. The thick black lines denote the median, and the boundaries of the boxes denote the interquartile range. Outliers are defined as data points more than 1.5 times the width of the interquartile range away from the 25th or 75th percentile.

Figure 3: At (a) US-UMB, (c) US-PFa, and (e) WCr, days experiencing a GLPF event and precipitation (P>0 mm) in June through August (light gray box plots) have significantly higher daily average temperatures relative to rainy days not experiencing a GLPF event (dark grey box plots), according to a t test of the difference between the population means. (b, d, f) The same is true on dry days (P=0 mm). In all panels, n indicates the number of days considered, and p is the p-value from the hypothesis test comparing the GLPF and non-GLPF days.

Figure 4: Daily June to August NEP residuals for GLPF (light gray box plots) and non-GLPF (dark gray box plots) days for days with no precipitation (P=0mm) and no severely limiting incoming shortwave radiation (R>200 W m^{-2}), with the linear relationship between NEP and R removed. ((a) US-UMB, (c) US-PFa, and (e) WCr) as well as with both the linear relationship with R and the linear relationship with temperature removed ((b) US-UMB, (d) US-PFa, and (f) WCr). For US-UMB and US-PFa, the difference between GLPF and non-GLPF days remains significant when removing the relationship with radiation, and the significance only disappears when the relationship with temperature is also eliminated, indicating that the NEP suppression is not due only to shortwave radiation effects.

Figure 5: All study sites showed comparable tendencies toward the suppression of net July through August carbon uptake during years of strong July GLPF activity. This is shown both (a) as a scatterplot of normalized mean July through August NEP versus the mean July GLPF membership coefficient (R^2 = 0.44) and (b) as a time series of the negative July GLPF overlain onto the time series of normalized mean July through August NEP (Panel (b)). This consistency suggests a region-wide suppression of forest net carbon uptake during the years in the study period during which the GLPF was particularly active during July. Vertical gray lines join NEP observations taken during the same year.

Figure 6: The seasonal component of the NEP time series shows that the years experiencing the lowest mean July through August NEP (dark green lines) showed an overall suppressed NEP seasonal peak compared to high-uptake years (light green lines), with differences between the time series often becoming evident before the start of July. This occurred for all sites (a: US-UMB; b: US-PFa; c: US-WCr). The year 2001 was not included because of the extreme effects of herbivory in this year.

Figure 1.

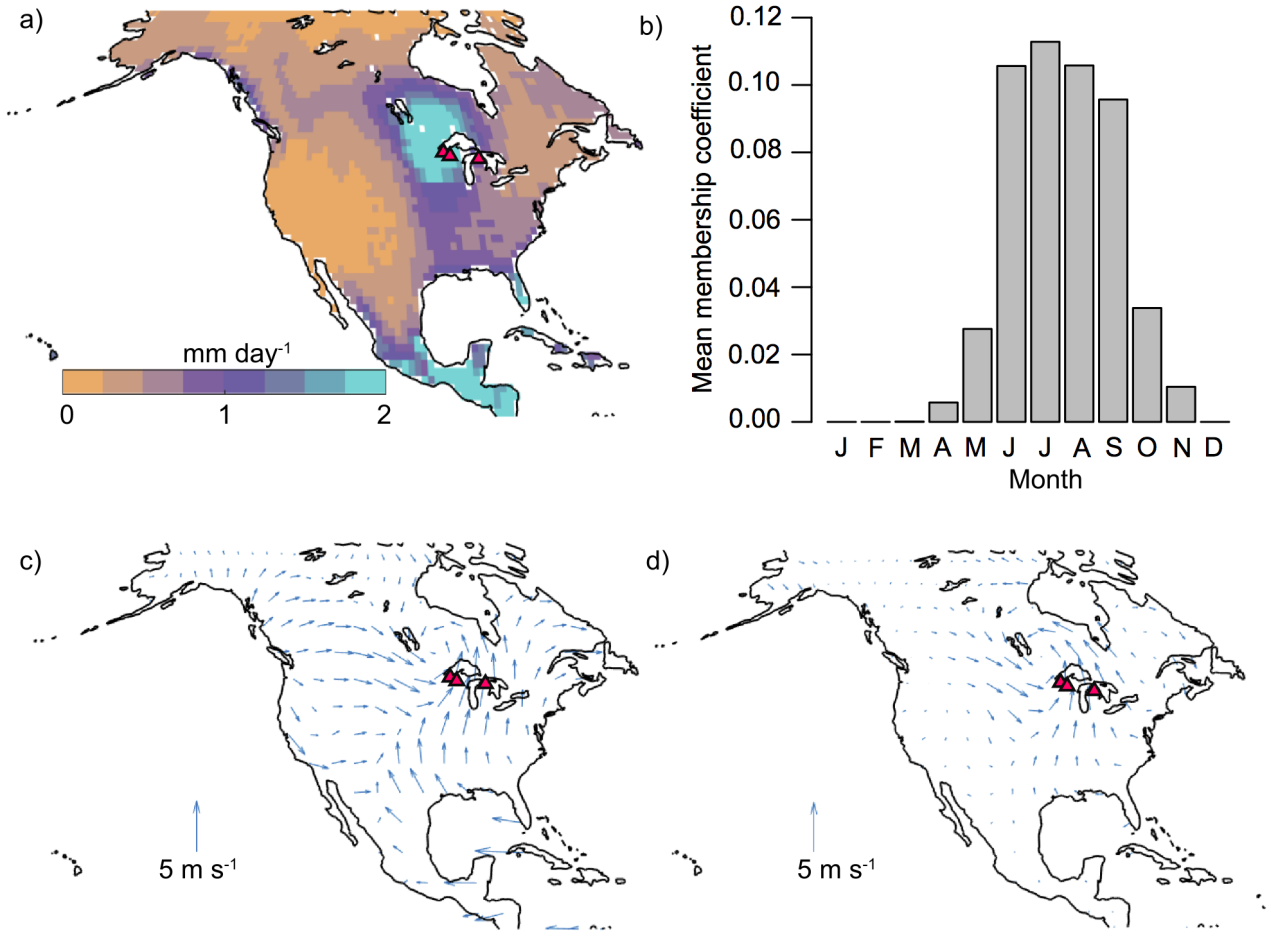
a)
mm day-1
0
1
2
b)
Mean membership coefficient
0.12
0.10
0.08
0.06
0.04
0.02
0.00
J F M A M J J A S O N D
Month
c)
5 m s-1
d)
5 m s-1

Figure 2.

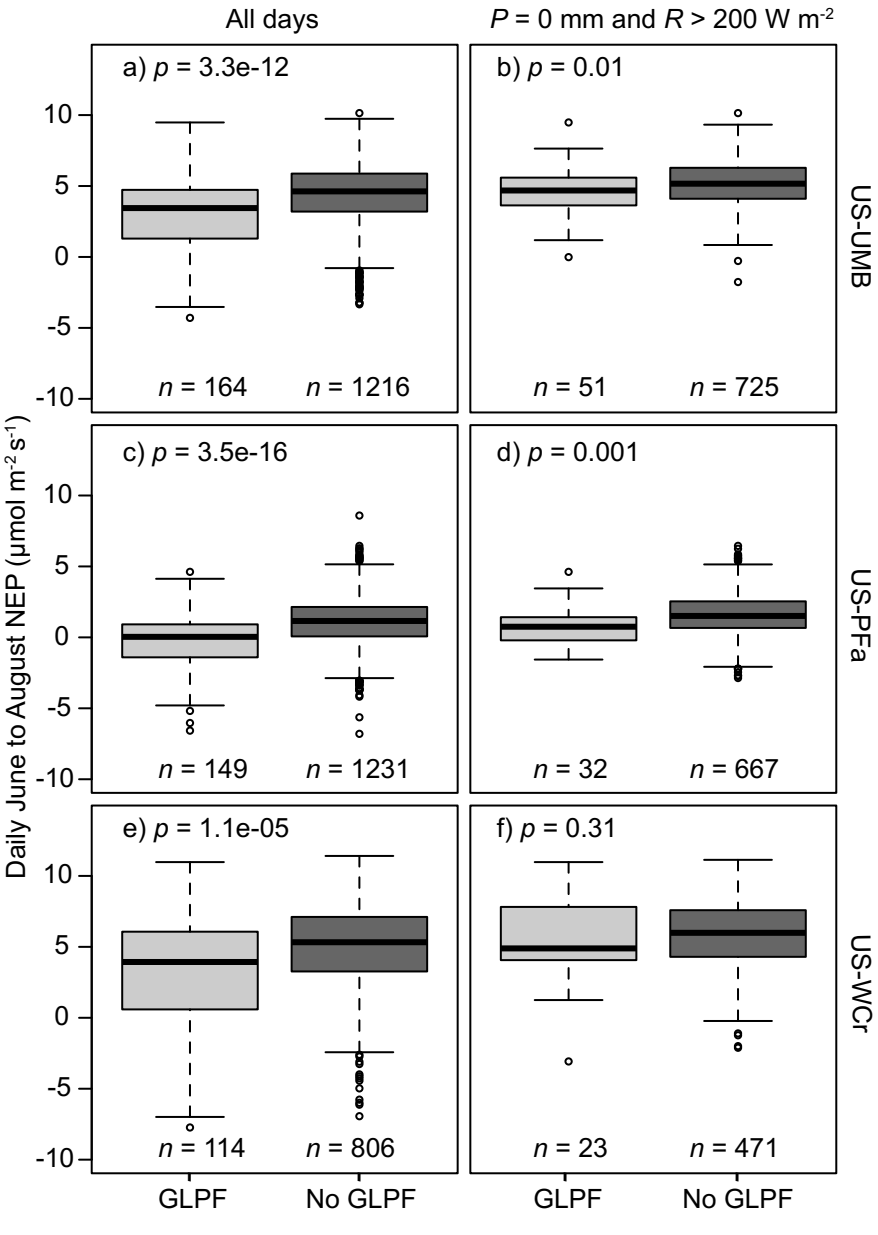
All days
P = 0 mm and R > 200 W m-2
a) p = 3.3e-12
b) p = 0.01
c) p = 3.5e-16
d) p = 0.001
e) p = 1.1e-05
f) p = 0.31
US-UMB
US-PFa
US-WCr
Daily June to August NEP (µmol m-2 s-1)
10
5
0
-5
-10
n = 164
n = 1216
n = 51
n = 725
n = 149
n = 1231
n = 32
n = 667
n = 114
n = 806
n = 23
n = 471
GLPF
No GLPF
GLPF
No GLPF

Figure 3.

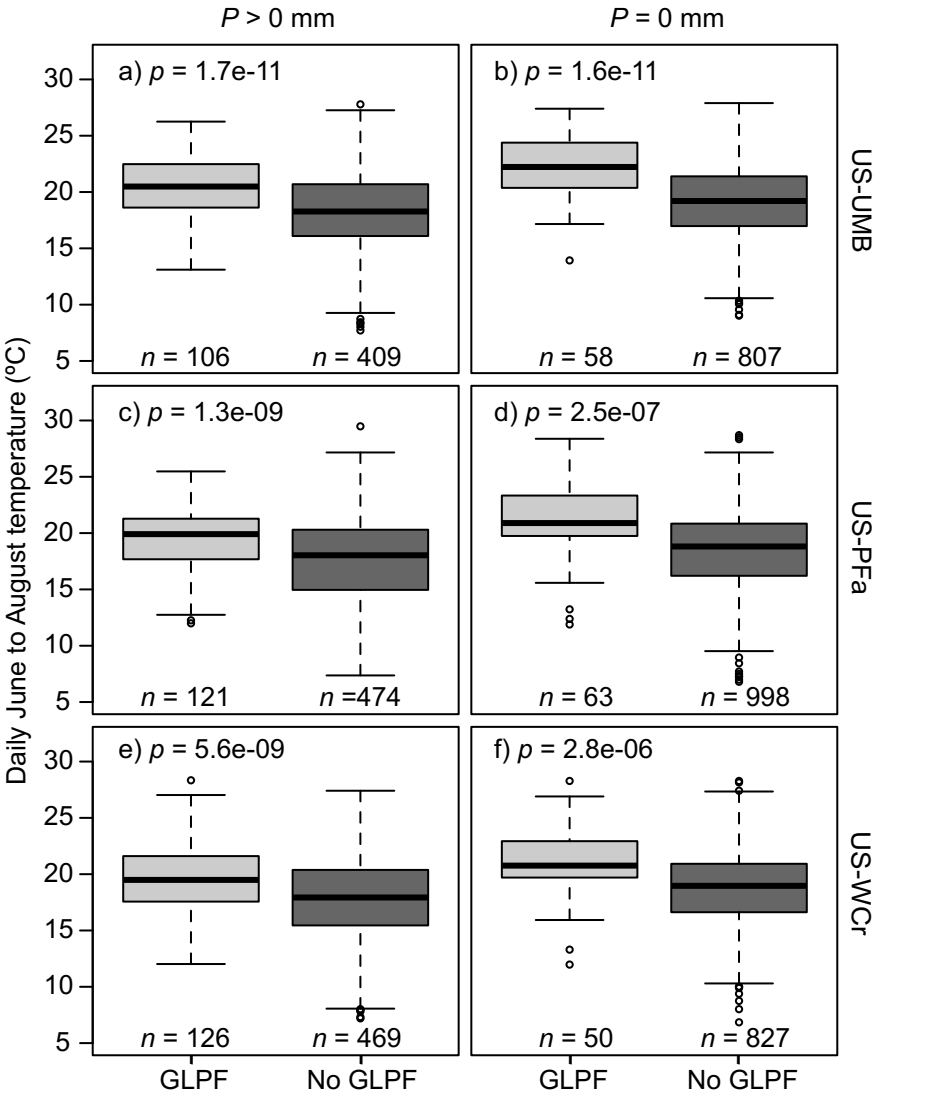
P > 0 mm
P = 0 mm
a) p = 1.7e-11
b) p = 1.6e-11
c) p = 1.3e-09
d) p = 2.5e-07
e) p = 5.6e-09
f) p = 2.8e-06
US-UMB
US-PFa
US-WCr
Daily June to August temperature (°C)
30
25
20
15
10
5
n = 106
n = 409
n = 58
n = 807
n = 121
n =474
n = 63
n = 998
n = 126
n = 469
n = 50
n = 827
GLPF
No GLPF
GLPF
No GLPF

Figure 4.

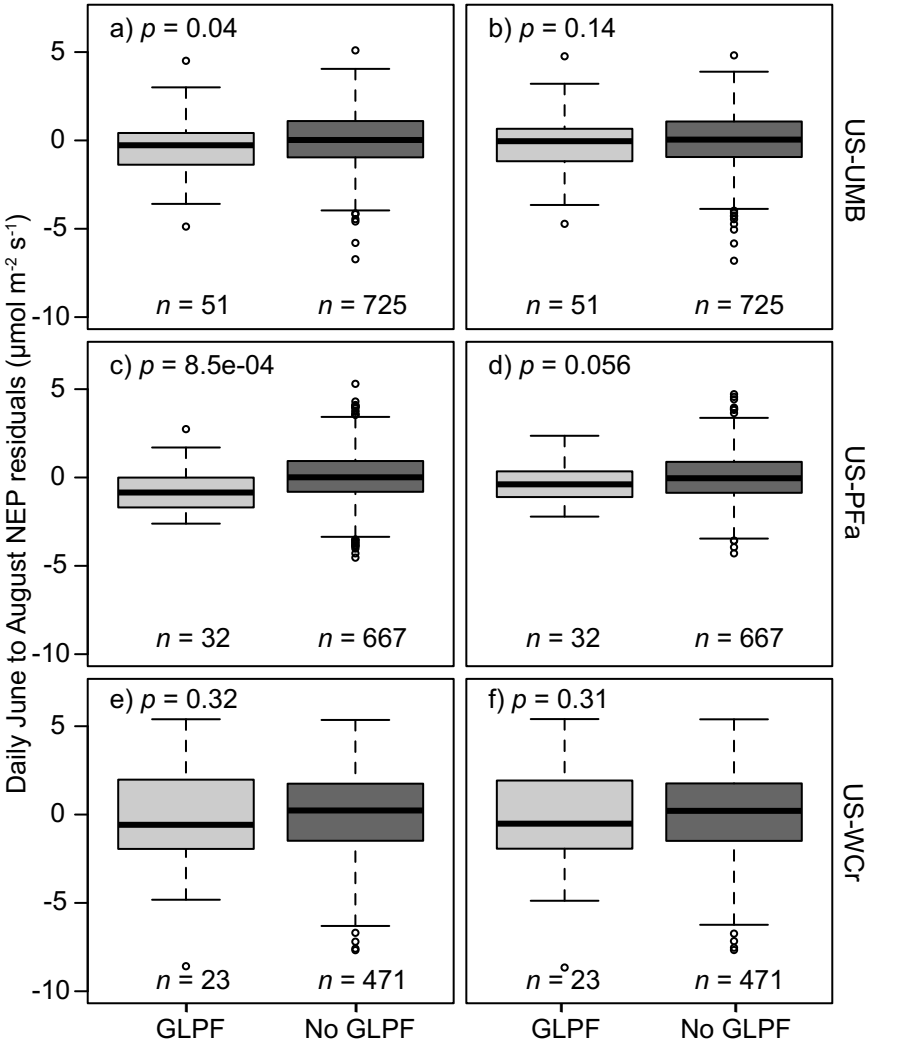
a) p = 0.04
b) p = 0.14
c) p = 8.5e-04
d) p = 0.056
e) p = 0.32
f) p = 0.31
n = 51
n = 725
n = 32
n = 667
n = 23
n = 471
US-UMB
US-PFa
US-WCr
Daily June to August NEP residuals (µmol m-2 s-1)
5
0
-5
-10
GLPF
No GLPF

Figure 5.

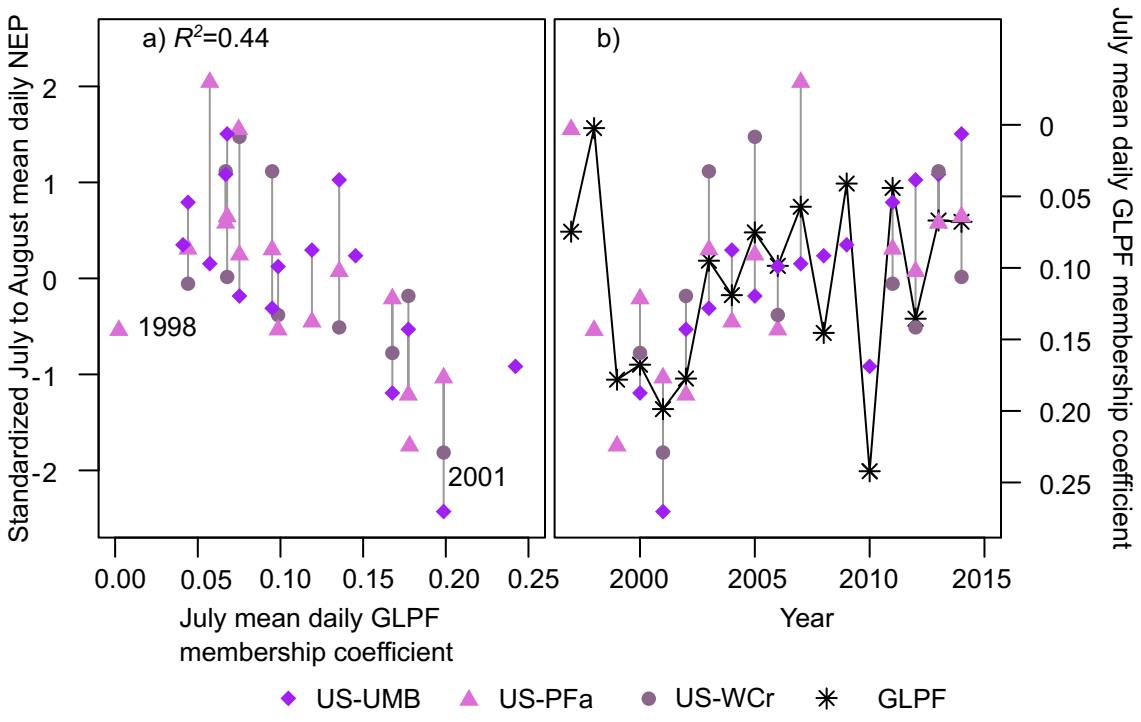
a) R^2=0.44
b)
1998
2001
Standardized July to August mean daily NEP
July mean daily GLPF membership coefficient
July mean daily GLPF membership coefficient
Year
US-UMB
US-PFa
US-WCr
GLPF

Figure 6.

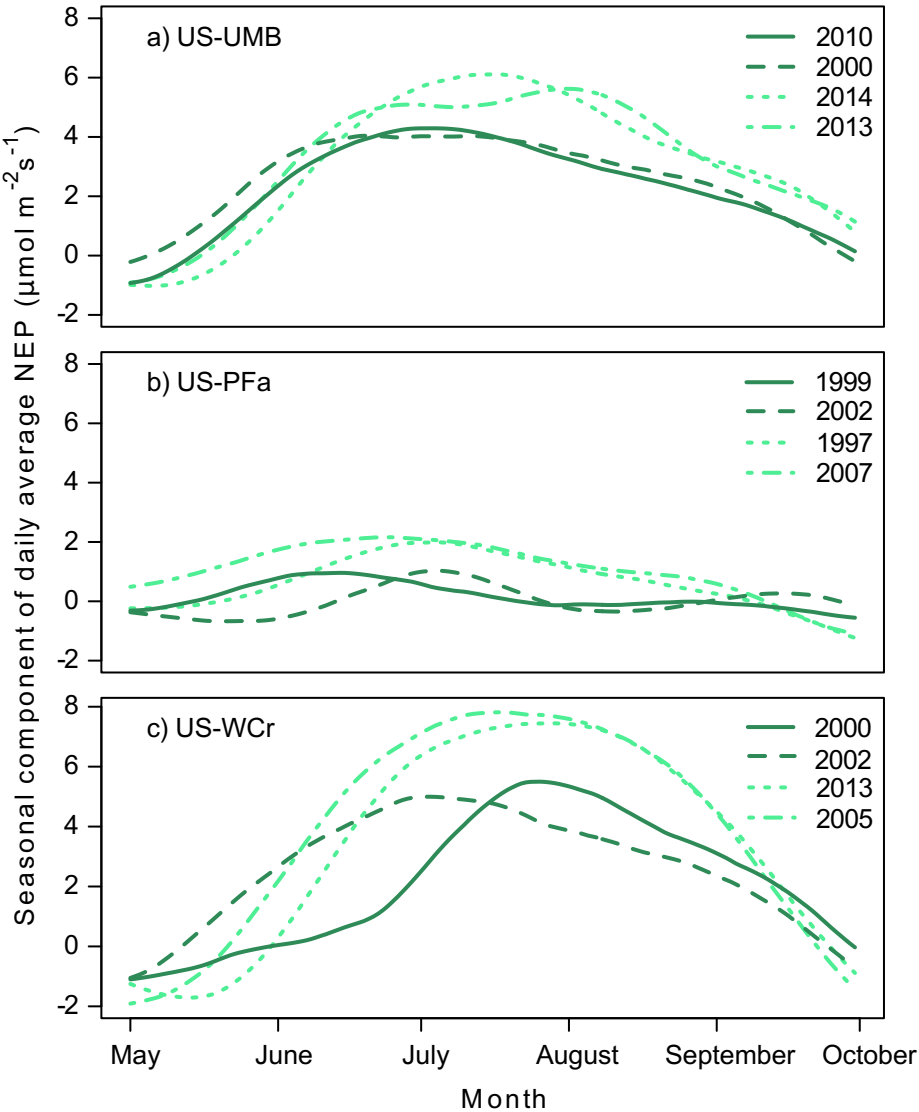
a) US-UMB
2010
2000
2014
2013
b) US-PFa
1999
2002
1997
2007
c) US-WCr
2000
2002
2013
2005
8
6
4
2
0
-2
Seasonal component of daily average NEP (µmol m-2s-1)
May
June
July
August
September
October
Month